



OPEN

Study of the heavily p-type doping of cubic GaN with Mg

C. A. Hernández-Gutiérrez¹✉, Y. L. Casallas-Moreno², Victor-Tapio Rangel-Kuoppa³, Dagoberto Cardona⁴, Yaoqiao Hu⁵, Yuri Kudriatsev⁶, M. A. Zambrano-Serrano⁷, S. Gallardo-Hernandez⁸ & M. Lopez-Lopez⁸✉

We have studied the Mg doping of cubic GaN grown by plasma-assisted Molecular Beam Epitaxy (PA-MBE) over GaAs (001) substrates. In particular, we concentrated on conditions to obtain heavy p-type doping to achieve low resistance films which can be used in bipolar devices. We simulated the Mg-doped GaN transport properties by density functional theory (DFT) to compare with the experimental data. Mg-doped GaN cubic epitaxial layers grown under optimized conditions show a free hole carrier concentration with a maximum value of $6 \times 10^{19} \text{ cm}^{-3}$ and mobility of $3 \text{ cm}^2/\text{Vs}$. Deep level transient spectroscopy shows the presence of a trap with an activation energy of 114 meV presumably associated with nitrogen vacancies, which could be the cause for the observed self-compensation behavior in heavily Mg-doped GaN involving Mg- V_N complexes. Furthermore, valence band analysis by X-ray photoelectron spectroscopy and photoluminescence spectroscopy revealed an Mg ionization energy of about 100 meV, which agrees quite well with the value of 99.6 meV obtained by DFT. Our results show that the cubic phase is a suitable alternative to generate a high free hole carrier concentration for GaN.

Gallium Nitride (GaN) in the wurtzite or hexagonal phase (h-GaN) has been intensively studied during the last decades for its unique properties. It has a large direct band gap with high saturation velocity, which makes it a promising candidate to achieve high power devices^{1–4}. However, spontaneous piezoelectric polarization occurs in h-GaN inducing internal electric fields, which causes energy band tilting⁵. These internal electric fields significantly influence optoelectronic devices' performance⁶. This is not the case for the much less explored zincblende or cubic phase of GaN (c-GaN). Due to the crystal symmetry of c-GaN, spontaneous piezoelectric polarization can be avoided, making it a more suitable material for the described applications⁷. At the same time, c-GaN offers additional advantages like; greater hole mobility and a smaller band gap of 3.2 eV at room temperature (RT) compared with 3.4 eV of h-GaN. This last characteristic is an extra advantage when alloying c-GaN with c-InN (with a bandgap of 0.66 eV at RT), as less In is required to achieve smaller band gaps^{8,9}. Regarding optoelectronic applications, there is a wider choice of cubic substrates to grow c-GaN, such as GaAs and SiC^{10,11}. Growing on these cubic substrates allows easier cleavage, enabling mirror-like edges suitable for laser applications. At the same time, the (001) oriented substrates induce natural stacking fault annihilation, as they propagate along 60° orientations¹¹. Moreover, employing Si- and/or GaAs-based substrates paves the way for the use of the well-developed device processing technology on these substrates. Due to these advantages, nitrides in the cubic phase are strong candidates to develop semiconductor devices such as LEDs and photovoltaic devices. However, c-GaN is metastable, causing its growth a difficult challenge¹². An additional drawback is that under typical growth conditions hexagonal GaN has an intrinsic n-type nature, and if GaN is aimed for optoelectronic applications, then the development of p-type doping of GaN is fundamental for any p–n junction-based device. To achieve p-type characteristics in h-GaN, Mg doping was proposed¹³. However, for Mg-doped h-GaN there

¹Tecnológico Nacional de México/Instituto Tecnológico de Tuxtla Gutiérrez, Posgrado en Ingeniería Grupo de Opto-mecatrónica, Carretera Panamericana km 1080, 29050 Tuxtla Gutiérrez, Mexico. ²CONACYT, Instituto Politécnico Nacional - UPIITA, Av. IPN 2580 Col. Barrio La Laguna Ticomán, Ciudad de México 07340, Mexico. ³Centro de Investigación en Dispositivos Semiconductores, Instituto de Ciencias, Universidad Autónoma de Puebla, Puebla 72000, Mexico. ⁴Facultad de Ciencias Físico-Matemáticas, UMSNH, Edificio L, Francisco J. Mujica S/N, Morelia, Michoacán 58000, Mexico. ⁵Department of Materials Science and Engineering, The University of Texas At Dallas, Richardson, TX 75080, USA. ⁶Departamento de Ingeniería Eléctrica SEES, Cinvestav-IPN, Ciudad de México 07360, Mexico. ⁷Programa de Doctorado en Nanociencias Y Nanotecnología, Cinvestav-IPN, Ciudad de México 07360, Mexico. ⁸Departamento de Física, Cinvestav-IPN, Ciudad de México 07360, Mexico. ✉email: chernandez@fis.cinvestav.mx; mlopezl@cinvestav.mx

are major issues, namely: (a) a large acceptor activation energy ≈ 200 – 265 meV, (b) Mg solubility limit around 10^{20} cm $^{-3}$, and (c) compensation by native defects^{14,15}.

On the other hand, for c-GaN, theoretical calculations have predicted ionization energies for Mg acceptors around 130 meV¹⁶, in contrast with experimental reports about 165 meV¹⁷ and 230 meV¹⁸. Despite these early studies have been done almost three decades ago, the mentioned metastability nature of c-GaN and the Mg doping drawbacks have caused disperse and limited information on the electrical properties of Mg-doped cubic GaN^{19–24}. Recently the authors in reference²⁵ reported a free hole concentration in the order of 10^{19} cm $^{-3}$ in c-GaN. No subsequent study could be found where hole concentration is in the order of 10^{19} cm $^{-3}$ or larger. Thus, further research is necessary to achieve a better understanding of the Mg doping of c-GaN. This paper intends to report a comprehensive study of cubic GaN doped with Mg, employing density functional theory (DFT) supported with the experimental techniques of x-ray photoelectron spectroscopy valence band maximum (XPS-VBM), deep level transient spectroscopy (DLTS), and photoluminescence spectroscopy (PL). With special emphasis on demonstrating that cubic GaN is suitable to achieve a high free hole concentration when doped with Mg under appropriate conditions. We extracted the Mg activation energy by two different techniques obtaining results that are quite close to the theoretical prediction.

DFT simulation. First-principles simulation was performed to gain insight into the hole mobility and Mg ionization energy level in cubic GaN. The simulation was conducted by DFT as implemented by VASP²⁶ using projected augmented wave (PAW)^{27,28} pseudopotentials. Perdew-Burke-Ernzerhof generalized gradient approximation (GGA-PBE) functional was employed to depict the exchange–correlation potential energy. For all calculations, an energy cutoff of 520 eV was adopted for plane wave basis expansion. Brillouin-zone integrations were performed based on the Gamma-centred Monkhorst–Pack k -point mesh, with a sampling density of 0.03 Å $^{-1}$. Structures were relaxed using the conjugate gradient (CG) method with the convergence criterion of the force on each atom less than 0.02 eV/Å. The converged energy criterion is 10^{-5} eV for electronic minimization. The mobility μ depends on the effective mass m^* through $\mu = e\tau/m^*$ where the relaxation time τ depends on different scattering mechanisms, and the effective mass was calculated according to the band structure dispersion relationship: $m^* = \hbar^2 / \frac{d^2E}{dk^2}$. Herein we took into account both phonons scattering and ionized impurity scattering. We computed scattering rates at a temperature of 300 K. Calculation details and procedure can be found elsewhere²⁹.

The point defect computations were performed using the supercell technique adopting $2 \times 2 \times 2$ supercells of the primitive cell to mimic the dilute doping condition while ensuring a reasonable computation cost. The defect states with the charge q were corrected using the Freysoldt scheme³⁰, as implemented in the PyCDT package³¹. The Freysoldt scheme leads to the calculated formation energies approaching to the dilute-defect limit and independent of the supercell size³². The formation energy of defect D in charged state q $E^f[D^q]$ can be written as³³

$$E^f[D^q] = E_{\text{def}}[D^q] - E_{\text{bulk}} - \sum n_i \mu_i + q(E_F + E_{\text{VBM}}) + E_{\text{corr}}[D^q]$$

where $E_{\text{def}}[D^q]$ is the energy of the supercell with defects, E_{bulk} is the energy of the perfect supercell without any defects, n_i indicates the number of the i th-atoms that have been added into ($n_i > 0$) or removed from ($n_i < 0$) the supercell and μ_i is the chemical potential of defective atoms. E_{VBM} is the energy of the valence band maximum (VBM), and E_F is the Fermi level referenced to E_{VBM} . The correction term $E_{\text{corr}}[D^q]$ is introduced to take into account the spurious interactions between the charges and their images.

Figure 1a shows the hole mobility as a function of doping concentration at 300 K for c-GaN. At low doping concentrations in the order of 10^{14} to 10^{16} cm $^{-3}$, the hole mobility is limited by the intrinsic phonon scattering, with an upper limit of 57.1 cm 2 /Vs. The mobility decreases with doping concentration down to a value of 6 cm 2 /Vs for a doping concentration of 10^{22} cm $^{-3}$. Cubic GaN shows a value of hole mobility around 18 cm 2 /Vs at a doping concentration of 5×10^{19} cm $^{-3}$, compared to the Hall measurement determined value of ~ 8 cm 2 /Vs (presented in the next sections) for this doping concentration. The difference could be accounted for by other factors, such as surface and interface (c-GaN/GaAs) scattering that were not considered in the present calculation but are expected to exist in real samples. Figure 1b shows the substituting Mg defect formation energy as a function of the Fermi level calculated under both N-rich and Ga-rich conditions. The Ga-rich condition leads to a higher defect formation energy, but the same charge state transition levels when compared with N-rich condition, which is similar to that in hexagonal GaN³⁴. The ionization energy level corresponds to the transition level at which the Mg charge state changes from 0 to -1 ($\epsilon(0/-1)$), which is about 99.6 meV above the valence band maximum (VBM) according to our DFT calculation, well consistent with our experimental determined value as will be discussed below. Our further calculation (Supplementary Fig. S1) also reveals an activation energy of 210 meV for Mg in hexagonal phase GaN, suggesting that p-type doping in cubic GaN could be enhanced due to the lower ionization energy in comparison with hexagonal GaN.

Samples preparation. Cubic GaN layers were grown by plasma-assisted molecular beam epitaxy (PAMBE) on semi-insulating GaAs (001) substrates. A Mg effusion cell was employed at temperatures (T_{Mg}) from 360 to 430 °C to produce high values of the Mg flux aiming to obtain heavy p-type doping. The substrate temperature (T_{Sub}) was varied between 670 and 700 °C, the N power between 100 and 150 W (with a fixed N flux of 0.4 sccm), depending on the sample (Table S1). The thickness of the samples was measured by cross-section SEM obtaining an average thickness of 400 nm (Fig. S2). The cubic phase structure was confirmed by x-ray diffraction (Fig. S3). Further details on the PAMBE growth and sample characteristics can be found in Supplementary Information.

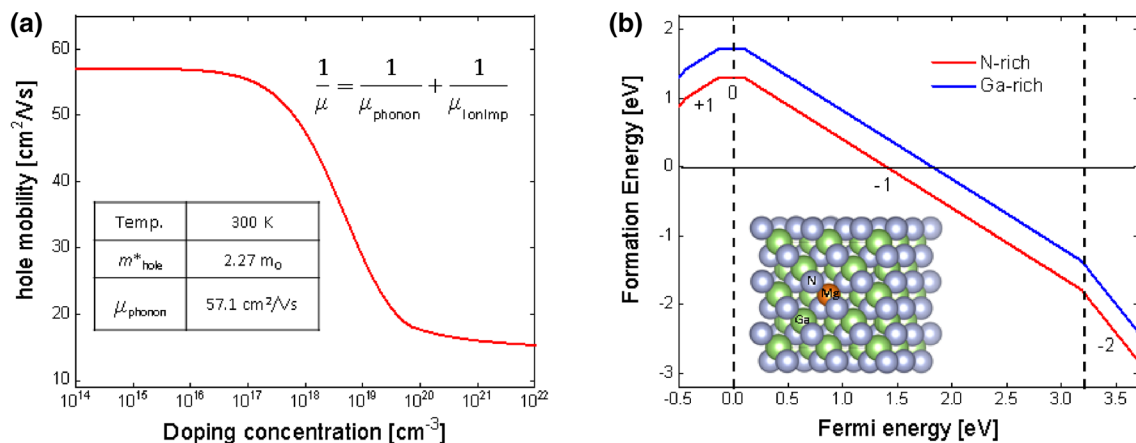


Figure 1. (a) Calculated hole mobility as a function of doping concentration in cubic GaN considering both phonons scattering and ionized impurities (IonImp) scattering. The temperature is set at $T=300$ K. The intrinsic phonon limited mobility, hole effective mass is also listed in the figure. (b) The calculated defect formation energy of Mg substitution for Ga as a function of Fermi energy. The zero of Fermi energy is aligned to the valence band edge. A negative Fermi energy means hole degenerate doping condition while Fermi level above conduction band edge means the electron degenerate doping condition. The ionization energy corresponds to the transition level $\epsilon(0/-1)$ which is about 99.6 meV above the VBM. Two conditions, i.e., N-rich and Ga-rich, are considered. The practical growth condition will fall in between these two extremes. An illustration of the atomic structure of Mg-doped cubic GaN is inserted in the figure.

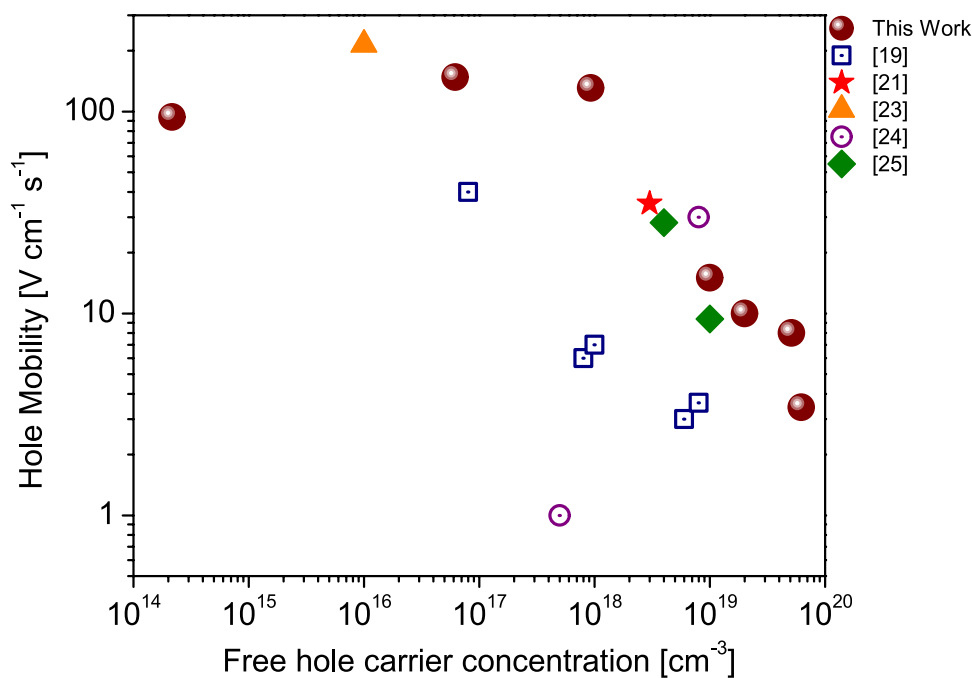


Figure 2. Hall effect mobility as a function of free hole carrier concentration. Our samples are represented by circles and are complemented with previously reported results for Mg-doped c-GaN^{19,21,23–25}.

Electrical characterization: Hall effect and DLTS analysis. Sample processing and measurement details for the electrical characterization are presented in Supplementary Information. The hole mobility of the samples as a function of hole concentration measured by the Hall effect is shown in Fig. 2. We included in the figure available data reported in the literature for Mg-doped cubic GaN; the hole concentration varies in the order of 10^{14} – 10^{19} cm^{-3} , whilst the mobility in the range of 148–1 cm^2/Vs . According to our XPS analysis, the samples with a high Nitrogen concentration (fewer Nitrogen vacancies V_N) presented an increase in hole carrier concentration, in good agreement with reference³⁵. The optimized growth conditions were Ga-rich with $\zeta_N / (\zeta_{Ga} + \zeta_{Mg}) \sim 0.9$, where ζ_N , ζ_{Ga} , and ζ_{Mg} are the concentration of N, Ga, and Mg, respectively. These growth con-

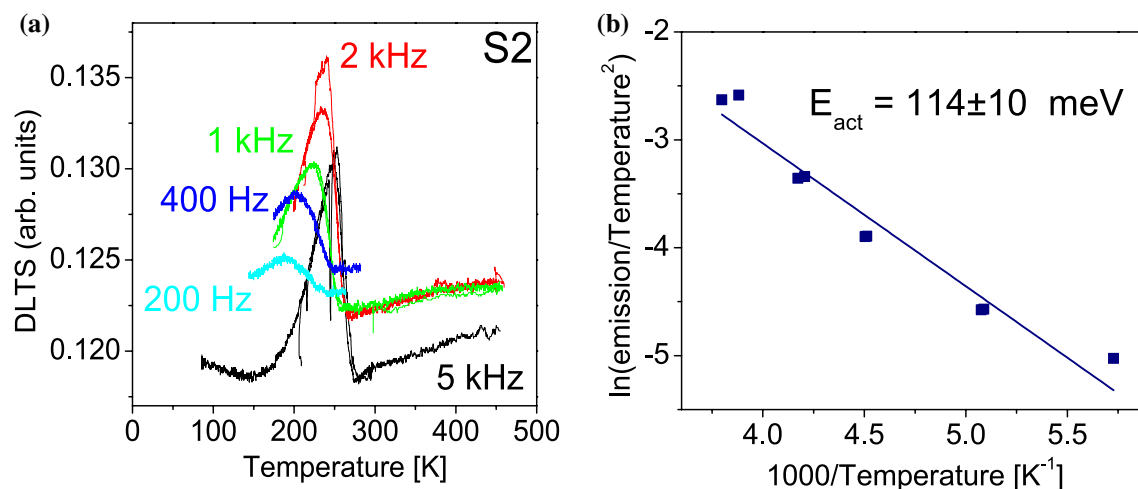


Figure 3. (a) DLTS spectra and (b) Arrhenius plot of sample S2.

ditions allowed us to achieve a high free hole carrier concentration in the range of $6 \times 10^{19} \text{ cm}^{-3}$ with a mobility value of $3.4 \text{ cm}^2/\text{Vs}$. To the best of our knowledge, the reported free hole concentration in this work is higher than previously reported up to now as is illustrated in Fig. 2. The mobility for samples with high hole concentration is lower than the DFT estimated mobility dominated by ionized impurities scattering, which suggests that other mechanisms, like surface and interface scattering, should be considered. The atomic Mg percentage in the sample with the highest hole concentration is 0.15% (extracted by XPS), which corresponds to a Mg concentration of $1.3 \times 10^{20} \text{ cm}^{-3}$. Therefore, if the free hole carrier concentration is around $6 \times 10^{19} \text{ cm}^{-3}$ then the ionization efficiency is 46%. We observed (Fig. S4) in our samples grown with very high Mg fluxes ($\text{BEP}_{\text{Mg}} > 10^{-8} \text{ Torr}$) a strong reduction in hole concentration. Under these growth conditions, Mg exceeds the doping range and its content approximates to the solubility saturation. Thus, Mg atoms might incorporate at places different from the expected Ga sites, and could generate donors causing a self-compensation effect, which would yield to a reduction of hole concentration. Note that a compensating behavior has been observed in hexagonal III-nitrides grown by MBE³⁶ and MOCVD³⁷. A model involving Mg-V_N complex was proposed to explain the self-compensation in heavily Mg-doped p-type h-GaN³⁸.

DLTS measurements were performed looking for carrier traps in our samples. The DLTS spectra of sample S2 are presented in Fig. 3, for each repetition rate. We observe a single defect level, the positive peak indicates a minority trap. As the repetition rate diminishes, the DLTS peak moves to lower temperatures, as expected. The emission at each peak maximum coincides with the emission of the deep level, yielding an emission vs absolute temperature dependence. An Arrhenius plot was done, using the standard procedure proposed by Lang³⁹, obtaining activation energy of $E_{\text{act}} = 114 \text{ meV}$. A deep level with an activation energy of 120 meV has been reported in hexagonal GaN, which was extracted from Arrhenius plots of DLTS measurements and assigned to V_N⁴⁰. For cubic GaN an N-vacancy related defect was obtained by DLTS with an activation energy of 200 meV⁴¹. These results and the fact that our samples were grown in Ga-rich conditions suggest that the level we observed with an energy $E_{\text{act}} = 114 \text{ meV}$ could be related to N vacancies. Therefore, the reduction in hole concentration for samples grown with $\text{BEP}_{\text{Mg}} > 10^{-8} \text{ Torr}$ could be related to a Mg-V_N complex, as above mentioned.

XPS valence band analysis and PL. From our DFT calculations, the energy difference between the valence band maximum and the Fermi level is about 99.6 meV. To extract the activation energy on sample S2, we employed the XPS valence band method (XPS-VBM)⁴². In Fig. 4a is observed that the energy difference between the valence band and Fermi level is 96.5 meV, which is very close to that predicted by DFT (99.6 meV). In addition, photoluminescence spectroscopy (PL) measurements were performed to obtain an independent estimation for the Mg acceptor activation energy. The PL measurements were carried out employing a He-Cd Laser and a CCD detector. Figure 4b shows the PL spectrum of the sample S2 at 270 K. Two main transitions were observed corresponding to excitonic transition (X) at 3.27 eV and free electron to the acceptor (e-A) at 3.2 eV, respectively. Therefore, the Mg activation energy is calculated employing the method reported in ref⁴³, and correcting the (e-A) peak position by $KT/2$ (being K the Boltzmann constant and T the absolute temperature)⁴⁴. The energy band diagram extracted by PL analysis is shown in the inset of Fig. 4b. Thus, the acceptor activation energy can be calculated as:

$$E_{\text{Mg}}(\text{eV}) = E_x + \varepsilon_b - E_{e-A} + KT/2$$

where $E_x = 3.27 \text{ eV}$ is the c-GaN excitonic transition, $\varepsilon_b = 0.025 \text{ eV}$ is the free exciton binding energy, $E_{e-A} = 3.2 \text{ eV}$ emission is the (e-A) transition, and $KT/2 = 0.011 \text{ eV}$ is the temperature correction for (e-A)⁴⁴. Thus, the Mg ionization energy extracted by PL is 106 meV which is quite close to the predicted by DFT. The low Mg activation energy in c-GaN can be understood by the atomic geometric structure. The in-plane N-Ga bond distance (1.966 Å) in the hexagonal phase is slightly shorter than that in the cubic phase (1.968 Å), which means that the

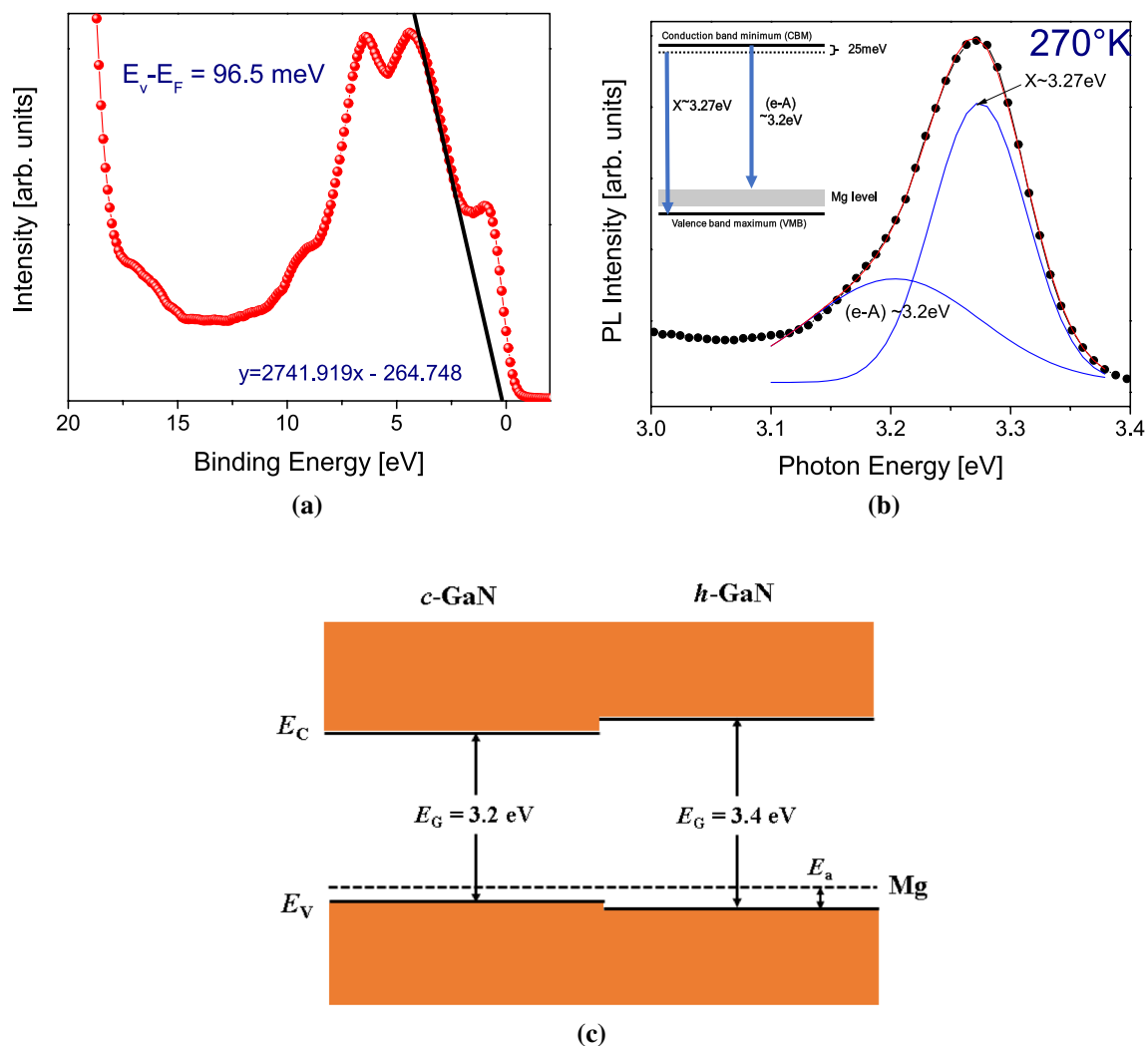


Figure 4. (a) Valence band analysis by XPS, (b) PL analysis at 270 K, and (c) schematic figure showing the band positions for c-GaN and h-GaN.

GaN bonding interaction in the hexagonal phase is stronger than the cubic phase. In terms of band alignment, the VBM of h-GaN lies lower than that of c-GaN, while the CBM of h-GaN lies higher than that of c-GaN. This also explains why h-GaN has a wider band gap than c-GaN. When both phases are doped with p-type Mg, the ionization energy level of Mg will be located closer to the VBM of c-GaN, as is illustrated in Fig. 4c.

Conclusions

We have studied the p-type doping in cubic phase GaN under a high flux of Mg atoms. First principles calculation under the DFT formalism was used to predict the transport properties of zincblende GaN and the Mg activation energy. The DFT Mg activation energy was found to be around 99.6 meV. This value matches quite accurately with the experimental results obtained by XPS-VBM and PL. A maximum hole concentration around $6 \times 10^{19} \text{ cm}^{-3}$ with mobility of $3.4 \text{ Vcm}^{-1} \text{ s}^{-1}$ was achieved. For higher Mg doping a self-compensation effect observed probably caused by Mg- V_N complexes.

Received: 25 June 2020; Accepted: 23 September 2020

Published online: 08 October 2020

References

- Chen, L. C., Hsu, C. Y., Lan, W. H. & Teng, S. Y. GaN-based light-emitting diodes with Ni/AuBe transparent conductive layer. *Solid. State. Electron.* **47**, 1843–1846. [https://doi.org/10.1016/S0038-1101\(03\)00129-1](https://doi.org/10.1016/S0038-1101(03)00129-1) (2003).
- Pearton, S. J. *et al.* GaN electronics for high power, high temperature applications. *Electrochem. Soc. Interface* **9**, 34–39. [https://doi.org/10.1016/S0921-5107\(00\)00767-4](https://doi.org/10.1016/S0921-5107(00)00767-4) (2000).
- Su, Y. K., Juang, F. S. & Chen, M. H. GaN metal-semiconductor-metal visible-blind photodetectors with transparent indium-tin-oxide contact electrodes. *Jpn. J. Appl. Phys. 1 Regul. Pap. Short Notes Rev. Pap.* **42**, 2257–2259. <https://doi.org/10.1143/JJAP42.2257> (2003).

4. Rangel-Kuoppa, V. T., Aguilar, C. G. & Sánchez-Reséndiz, V. Structural, optical and electrical study of undoped GaN layers obtained by metalorganic chemical vapor deposition on sapphire substrates. *Thin Solid Films* **519**, 2255–2261. <https://doi.org/10.1016/j.tsf.2010.10.053> (2011).
5. Yu, E. T., Dang, X. Z., Asbeck, P. M., Lau, S. S. & Sullivan, G. J. Spontaneous and piezoelectric polarization effects in III–V nitride heterostructures. *J. Vac. Sci. Technol. B Microelectron. Nanom. Struct.* **17**, 1742. <https://doi.org/10.1116/1.590818> (1999).
6. Wang, J., Wang, L., Zhao, W., Hao, Z. & Luo, Y. Understanding efficiency droop effect in InGaN/GaN multiple-quantum-well blue light-emitting diodes with different degree of carrier localization. *Appl. Phys. Lett.* **97**, 11–14. <https://doi.org/10.1063/1.3520139> (2010).
7. As, D. J. & Mietze, C. MBE growth and applications of cubic AlN/GaN quantum wells. *Phys. Status Solidi Appl. Mater. Sci.* **210**, 474–479. <https://doi.org/10.1002/pssa.201200653> (2013).
8. Lee, L. Y. Cubic zincblende gallium nitride for green-wavelength light-emitting diodes. *Mater. Sci. Technol. (UK)* **33**, 1570–1583. <https://doi.org/10.1080/02670836.2017.1300726> (2017).
9. Rangel-Kuoppa, V. T., Suihkonen, S., Sopenan, M. & Lipsanen, H. Metal contacts on InN: proposal for Schottky contact. *Jpn. J. Appl. Phys. 1 Regul Pap. Short Notes Rev. Pap.* **45**, 36–39. <https://doi.org/10.1143/JJAP.45.36> (2006).
10. Strite, S. et al. An investigation of the properties of cubic GaN grown on GaAs by plasma-assisted molecular-beam epitaxy. *J. Vac. Sci. Technol. B Microelectron. Nanom. Struct.* **9**, 1924–1929. <https://doi.org/10.1116/1.585381> (1991).
11. Gamez-Cuatzin, H. et al. Electroluminescence characterization of cubic gallium nitride p-n junctions grown on SiC/Si substrates by MBE. *Phys. Status Solidi Appl. Res.* **176**, 131–135. [https://doi.org/10.1002/\(SICI\)1521-396X\(199911\)176:1%3c131::AID-PSSA131%3e3.0.CO;2-D](https://doi.org/10.1002/(SICI)1521-396X(199911)176:1%3c131::AID-PSSA131%3e3.0.CO;2-D) (1999).
12. Casallas-Moreno, Y. L. et al. As 4 overpressure effects on the phase purity of cubic GaN layers grown on GaAs substrates by RF-MBE. *Appl. Surf. Sci.* **353**, 588–593. <https://doi.org/10.1016/j.apsusc.2015.06.054> (2015).
13. Amano, H. Growth of GaN on sapphire via low-temperature deposited buffer layer and realization of p-type GaN by Mg doping followed by low-energy electron beam irradiation (Nobel Lecture). *Ann. Phys.* **527**, 327–333. <https://doi.org/10.1103/RevModPhys.87.1133> (2015).
14. Van De Walle, C. G. & Neugebauer, J. First-principles calculations for defects and impurities: applications to III-nitrides. *J. Appl. Phys.* **95**, 3851–3879. <https://doi.org/10.1063/1.1682673> (2004).
15. Wang, H. & Chen, A. B. Calculations of acceptor ionization energies in GaN. *Phys. Rev. B Condens. Matter Mater. Phys.* **63**, 1252121–1252127. <https://doi.org/10.1103/PhysRevB.63.125212> (2001).
16. Mireles, F. & Ulloa, S. E. Acceptor binding energies in GaN and AlN. *Mater. Res. Soc. Symp. Proc.* **482**, 839–844. <https://doi.org/10.1103/PhysRevB.58.3879> (1997).
17. Akasaki, I., Amano, H., Kito, M. & Hiramatsu, K. Photoluminescence of Mg-doped p-type GaN and electroluminescence of GaN p-n junction LED. *J. Lumin.* **4849**, 666–670. [https://doi.org/10.1016/0022-2313\(91\)90215-H](https://doi.org/10.1016/0022-2313(91)90215-H) (1991).
18. As, D. J. et al. Incorporation and optical properties of magnesium in cubic GaN epilayers grown by molecular beam epitaxy. *Appl. Phys. Lett.* **73**, 1835–1837. <https://doi.org/10.1063/1.122298> (1998).
19. Lin, M. E., Xue, G., Zhou, G. L., Greene, J. E. & Morkoç, H. P-type zinc-blende GaN on GaAs substrates. *Appl. Phys. Lett.* **63**, 932–933. <https://doi.org/10.1063/1.109848> (1993).
20. As, D. J. et al. p- and n-type cubic GaN epilayers on GaAs. *Phys. Rev. B Condens. Matter Mater. Phys.* **54**, R11118–R11121. <https://doi.org/10.1103/PhysRevB.54.R11118> (1996).
21. Martinez-Guerrero, E. et al. p and n type doping of cubic GaN on SiC (001). *Mater. Sci. Eng. B Solid State Mater. Adv. Technol.* **82**, 59–61. [https://doi.org/10.1016/S0921-5107\(00\)00719-4](https://doi.org/10.1016/S0921-5107(00)00719-4) (2001).
22. Paisley, M. J., Sitar, Z., Posthill, J. B. & Davis, R. F. Growth of cubic phase gallium nitride by modified molecular-beam epitaxy. *J. Vac. Sci. Technol. A Vacuum Surf. Film.* **7**, 701–705. <https://doi.org/10.1116/1.575869> (1989).
23. As, D. J. Electrical and optical properties of Mg doped MBE grown cubic GaN epilayers. *Phys. Status Solidi Basic Res.* **210**, 445–449. [https://doi.org/10.1002/\(SICI\)1521-3951\(199812\)210:2%3c445::AID-PSSB445%3e3.0.CO;2-P](https://doi.org/10.1002/(SICI)1521-3951(199812)210:2%3c445::AID-PSSB445%3e3.0.CO;2-P) (1998).
24. Vilchis, H. & Sánchez-R, V. M. Electrical behavior of Mg doped cubic GaN on c-GaN structure. *Mater. Sci. Semicond. Process.* **37**, 68–72. <https://doi.org/10.1016/j.mssp.2015.01.052> (2015).
25. Compeán-García, V. D. et al. Effects of Mg incorporation in cubic GaN films grown by PAMBE near Ga rich conditions. *Mater. Sci. Semicond. Process.* **93**, 196–200. <https://doi.org/10.1016/j.mssp.2018.12.019> (2019).
26. Kresse, G. & Furthmüller, J. Efficient iterative schemes for ab initio total-energy calculations using a plane-wave basis set. *Phys. Rev. B Condens. Matter Mater. Phys.* **54**, 11169–11186. <https://doi.org/10.1103/PhysRevB.54.11169> (1996).
27. Kresse, G. & Hafner, J. Norm-conserving and ultrasoft pseudopotentials for first-row and transition elements. *J. Phys. Condens. Matter* **6**, 8245–8257. <https://doi.org/10.1088/0953-8984/6/40/015> (1994).
28. Kresse, G. & Joubert, D. From ultrasoft pseudopotentials to the projector augmented-wave method. *Phys. Rev. B Condens. Matter Mater. Phys.* **59**, 1758–1775. <https://doi.org/10.1103/PhysRevB.59.1758> (1999).
29. Hu, Y. et al. First principles calculations of intrinsic mobilities in tin-based oxide semiconductors SnO, SnO₂, and Ta₂SnO₆. *J. Appl. Phys.* **10**(1063/1), 5109265 (2019).
30. Freysoldt, C., Neugebauer, J. & Van de Walle, C. G. Electrostatic interactions between charged defects in supercells. *Phys. Status Solidi Basic Res.* **248**, 1067–1076. <https://doi.org/10.1002/pssb.201046289> (2011).
31. Broberg, D. et al. PyCDT: A Python toolkit for modeling point defects in semiconductors and insulator. *Comput. Phys. Commun.* **226**, 165. <https://doi.org/10.1016/j.cpc.2018.01.004> (2018).
32. Komsa, H. P., Rantala, T. T. & Pasquarello, A. Finite-size supercell correction schemes for charged defect calculations. *Phys. Rev. B Condens. Matter Mater. Phys.* **86**, 1–16. <https://doi.org/10.1103/PhysRevB.86.045112> (2012).
33. Zhang, S. B. & Northrup, J. E. Chemical potential dependence of defect formation energies. *Phys. Rev. Lett.* **67**, 2339–2342. <https://doi.org/10.1103/PhysRevLett.67.2339> (1991).
34. Zhong, H. X. et al. Reducing Mg acceptor activation-energy in Al_{0.83}Ga_{0.17}N disorder alloy substituted by nanoscale (AlN)/GaN superlattice using MgGa δ-doping: Mg local-structure effect. *Sci. Rep.* **4**, 1–6. <https://doi.org/10.1038/srep06710> (2014).
35. Fischer, A. M. et al. Origin of high hole concentrations in Mg-doped GaN films. *Phys. Status Solidi Basic Res.* **254**, 1–6. <https://doi.org/10.1002/pssb.201600668> (2017).
36. Gherasoiu, I., Yu, K. M., Reichertz, L. A. & Walukiewicz, W. InGaN doping for high carrier concentration in plasma-assisted molecular beam epitaxy. *Phys. Status Solidi Curr. Top. Solid State Phys.* **11**, 381–384. <https://doi.org/10.1002/pssc.201300460> (2014).
37. Qi, H. R. et al. The self-compensation effect of heavily Mg doped p-GaN films studied by SIMS and photoluminescence. *Superlattices Microstruct.* **133**, 106177. <https://doi.org/10.1016/j.spmi.2019.106177> (2019).
38. Kaufmann, U., Schlotter, P., Obloh, H., Köhler, K. & Maier, M. Hole conductivity and compensation in epitaxial GaN: Mg layers. *Phys. Rev. B Condens. Matter Mater. Phys.* **62**, 10867–10872. <https://doi.org/10.1103/PhysRevB.62.10867> (2000).
39. Lang, D. V. Deep-level transient spectroscopy: a new method to characterize traps in semiconductors. *J. Appl. Phys.* **45**, 3023–3032. <https://doi.org/10.1063/1.1663719> (1974).
40. Castaldini, A., Cavallini, A. & Polenta, L. Deep levels and irradiation effects in n-GaN. *J. Phys. Cond. Matter.* **12**, 10161. <https://doi.org/10.1088/0953-8984/12/49/315> (2000).
41. Fang, Z.-Q. et al. Deep centers in n-GaN grown by reactive molecular beam epitaxy. *Appl. Phys. Lett.* **72**, 2277. <https://doi.org/10.1063/1.121274> (1998).

42. Nayak, S. K., Gupta, M. & Shivaprasad, S. M. Structural, optical and electronic properties of a Mg incorporated GaN nanowall network. *RSC Adv.* **7**, 25998–26005. <https://doi.org/10.1039/c7ra02315d> (2017).
43. As, D. J. *et al.* The near band edge photoluminescence of cubic GaN epilayers. *Appl. Phys. Lett.* **70**, 1311–1313. <https://doi.org/10.1063/1.118521> (1997).
44. Xu, D., Yang, H., Zhao, D. G., Li, S. F. & Wu, R. H. Room-temperature optical transitions in Mg-doped cubic GaN/GaAs(100) grown by metalorganic chemical vapor deposition. *J. Appl. Phys.* **87**, 2064–2066. <https://doi.org/10.1063/1.372139> (2000).

Acknowledgments

The financial support by CONACyT (México), in particular project “RCUK-CONACyT 2016 FONCICYT/68” and Prodep Fortalecimiento de CA, Clave: CINVESTAV-CA-15 is gratefully acknowledged. Carlos Hernández wants to thank to CONACyT for PhD and Postdoctoral scholar ship. Moreover, we want to thank to Angel Guillen for SEM-EDS measurements.

Author contributions

C.A.H.-G. did simulation work, optical characterizations, and wrote the manuscript. Y.L.C.-M. did experimental work and analyzed the results. V.-T.R.-K. did DLTS measurements and wrote the manuscript. D.C. did experimental work. Y.H. simulation work. Y.K. analyzed the results. M.A. Z.-S. did experimental work and electrical characterization. S.G.-H. analyzed the results. M. L.-L. analyzed the results and wrote the manuscript. All authors reviewed the manuscript.

Competing interests

The authors declare no competing interests.

Additional information

Supplementary information is available for this paper at <https://doi.org/10.1038/s41598-020-73872-w>.

Correspondence and requests for materials should be addressed to C.A.H.-G. or M.L.-L.

Reprints and permissions information is available at www.nature.com/reprints.

Publisher’s note Springer Nature remains neutral with regard to jurisdictional claims in published maps and institutional affiliations.



Open Access This article is licensed under a Creative Commons Attribution 4.0 International License, which permits use, sharing, adaptation, distribution and reproduction in any medium or format, as long as you give appropriate credit to the original author(s) and the source, provide a link to the Creative Commons licence, and indicate if changes were made. The images or other third party material in this article are included in the article’s Creative Commons licence, unless indicated otherwise in a credit line to the material. If material is not included in the article’s Creative Commons licence and your intended use is not permitted by statutory regulation or exceeds the permitted use, you will need to obtain permission directly from the copyright holder. To view a copy of this licence, visit <http://creativecommons.org/licenses/by/4.0/>.

© The Author(s) 2020